PERGAMON

Chemical Engineering Science 55 (2000) 2653–2661

Chemical Engineering Science

Buoyancy-induced flows and phase-change heat transfer in a vertical capillary structure with symmetric heating

T. S. Zhao[a,*], P. Cheng[a], C. Y. Wang[b]

[a]*Department of Mechanical Engineering, The Hong Kong University of Science & Technology, Clear Water Bay, Kowloon, Hong Kong*
[b]*Department of Mechanical Engineering, The Pennsylvania State University, University Park, PA 16802, USA*

Received 4 March 1999; received in revised form 11 October 1999; accepted 15 October 1999

Abstract

This paper presents a numerical solution of a buoyancy-induced flow and phase-change heat transfer in a vertical porous channel heated symmetrically along its vertical walls. A multiphase mixture model that accounts for complex, interacting physical phenomena such as phase change, capillary action, buoyancy-induced flow convection in the subcooled liquid and multi-dimensional effects was used. It is found that for both single and the two-phase flow with a rather low vapor fraction, the induced mass flux increases as the applied heat flux is increased. However, as the vapor fraction is increased, the numerical results show that the induced mass flux drops drastically and remains approximately constant afterwards. This result agrees qualitatively with our previous experimental study on phase-change heat transfer in a heated vertical porous tube (Zhao et al., 1998. *ASME Journal of Heat Transfer*, *121*(3) 646–652). In this paper, the underlying mechanism leading to this interesting behavior is explained based on the liquid saturation distributions as well as the velocity fields for both vapor and liquid in the porous column.

Keywords: Porous media; Phase change; Heat transfer; Multiphase flow; Buoyancy-induced flow; Capillary-driven flow

1. Introduction

Phase-change heat transfer in porous media occurs in a number of technological applications, such as thermal energy storage, geothermal systems, porous medium heat pipes, food drying, porous insulation moisture transport, and post-accident analysis of liquid-cooled nuclear reactors, etc. (Wang & Cheng, 1997). In many of these systems, the effective pore radii are small, and both gravity and capillary effects are significant. One of the typical examples is depicted in Fig. 1, where a capillary structure subjected to a symmetric heating load is initially saturated with a subcooled liquid, supplied by an adjacent liquid pool. When the heat flux on the vertical walls is sufficiently large, a liquid–vapor two-phase zone forms adjacent to the walls, with the pure liquid zone existing elsewhere. In such a system, the subcooled liquid will be continuously pumped into the packed channel due to both buoyancy and capillary pressure effects.

Traditionally, analyses of two-phase flow in porous media are based on the assumption that vapor and the liquid phases are treated as distinct and separate fluids. The motion of each phase is described by the generalized Darcy's law in which a relative permeability is introduced to account for a decrease in effective flow cross-section due to the presence of the other phase (Bear, 1972). Unfortunately, the resulting equations with gravity, capillary and multi-dimensional effects taken into consideration, are not convenient for numerical solutions due to the large number of differential equations that must be solved. Moreover, the presence of a moving and irregular interface between the single- and two-phase regions adds more difficulties in the numerical solution, which requires an interface tracking procedure such as complex coordinate mapping or numerical remeshing (Ramesh & Torrance, 1990). These difficulties can be avoided in the recently developed multiphase mixture model (Wang, Beckermann & Fan, 1993). This new formulation unifies the governing equations for the single- and two-phase regions, and thus eliminates the need to track the moving liquid–vapor interface. Using this model, numerical solutions have been obtained for the study of natural convection boiling in a porous cavity heated from below

* Corresponding author. Tel.: 00852-2358-8647; fax: 00852-2358-1543.
E-mail address: metzhao@ust.hk (T. S. Zhao).

0009-2509/00/$ - see front matter
PII: S0009-2509(99)00530-8

Nomenclature

c	specific heat, J/(kg K)
$D(s)$	capillary diffusion coefficient, m^2/s
$f(s)$	hindrance function
g	gravitational acceleration, m/s^2
h	enthalpy, J/kg
h_{fg}	latent heat of liquid/vapor phase change, J/kg
H	pseudo-mixture enthalpy, J/m^3
j	diffusive mass flux, $kg/(m^2\ s)$
J(s)	capillary pressure function
k_r	relative permeability
k_{eff}	effective thermal conductivity, W/(m K)
K	absolute permeability, m^2
L	height of the capillary structure, mm
m''	liquid mass flux at the inlet, $kg/(m^2\ s)$
p	pressure, Pa
q''	imposed heat flux, W/m^2
s	liquid saturation
T	temperature, K
u	superficial or Darcian velocity vector, m/s
W	width of the capillary structure, mm
x	coordinate in horizontal direction
y	coordinate in vertical direction

Greek letters

β	thermal expansion coefficient
γ_h	two-phase advection correction coefficient
Γ_h	effective thermal diffusion coefficient, m^2/s
$\Delta\rho$	density difference ($=\rho_l-\rho_v$), kg/m^3
ε	porosity
λ	relative mobility
μ	viscosity, Pa s
ν	kinetic viscosity, m^2/s
ρ	density, kg/m^3
σ	surface tension, N/m
Ω	effective heat capacitance ratio

Subscripts

c	capillary
h	heating
ir	irreducible
k	'kinetic' property
l	liquid phase
s	solid phase
sat	saturated state
v	vapor phase

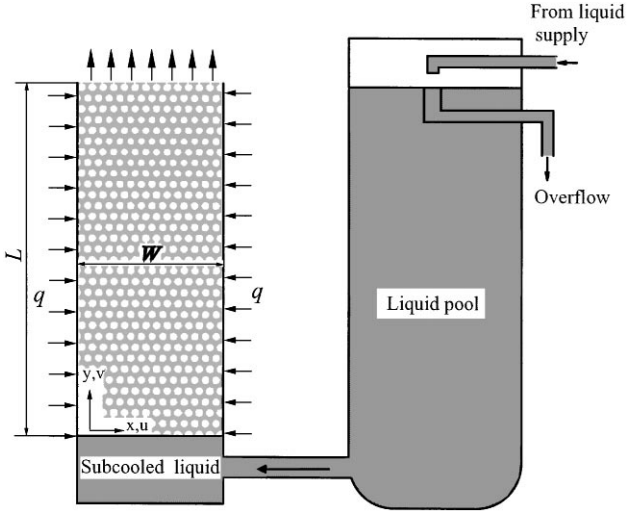

Fig. 1. Schematic of the physical problem and the coordinate system.

(Wang, Beckermann & Fan, 1994) and forced convection boiling in a horizontal porous channel with either localized heating from below (Easterday, Wang & Cheng, 1995) or symmetrical heating along a horizontal channel (Peterson & Chang, 1998). This model was also used to simulate the capillary evaporator of a capillary pumped loop (Wang, 1996).

In this work, a buoyancy-induced flow and phase-change heat transfer in a vertical porous channel heated symmetrically, as shown in Fig. 1, will be numerically solved based on the multiphase mixture model (Wang et al., 1993). The main objective is to provide a qualitative and quantitative understanding of the flow field and the associated heat transfer process in such a system. The most interesting feature of the present problem is the behavior of the induced mass flux as a function of the applied heat flux. For both single- and the two-phase flow with a rather low vapor fraction, the induced mass flux increases as the applied heat flux is increased. However, as the heat flux is increased, the induced mass flux drops drastically and then remains relatively constant afterwards. The effect of particle diameter on the dryout heat flux is also investigated.

2. Formulation

Consider a two-dimensional vertical capillary porous medium structure ($W\times L$) with symmetric heating at both lateral sides, as depicted in Fig. 1. The upper boundary is permeable while the lower boundary is connected to an adjacent liquid pool, where the water level can be maintained by controlling the mass balance between the liquid supply and the overflow. The capillary structure is initially filled with a subcooled liquid. As heat is added to the vertical walls, the liquid is continuously pumped into the packed column from the liquid pool due to the buoyancy effect. When the heat flux exceeds a certain value, evaporation occurs in the vicinity of the vertical

heated surfaces and extends to the neighboring region. As a consequence, a two-phase region consisting simultaneously of liquid and vapor is formed adjacent to the walls. Under this situation, the liquid/vapor meniscus inside the two-phase region can create a wicking effect to pump the subcooled liquid from the liquid pool into the packed structure, in addition to the buoyancy effect. This thermally driven flow involves a number of interacting phenomena, such as phase change, capillary action, thermal convection in both the subcooled liquid zone and the two-phase zone, and multi-dimensional effects. As will be given below, these effects are incorporated in the multiphase mixture model (Wang et al., 1993). The major assumptions and simplifications in this analysis include:

(1) the porous medium is rigid, uniform, isotropic and fully saturated with fluid;
(2) Darcy's law is applicable to both liquid and vapor phases;
(3) thermal dispersion is neglected;
(4) the thermophysical properties of both solid and fluid are assumed to be constant;
(5) the vapor, liquid and solid phases are in local thermal equilibrium;
(6) natural convection in the subcooled liquid region is considered and the Boussinesq approximation is invoked.

With the aforementioned assumptions and simplifications taken into account, the governing equations are (Wang et al., 1993).

Conservation of mixture mass:

$$\varepsilon \frac{\partial \rho}{\partial t} + \nabla\cdot(\rho \mathbf{u}) = 0 \tag{1}$$

Conservation of mixture momentum:

$$\mathbf{u} = -\frac{K}{\mu}[\nabla p - (\rho_k - \rho_o)\mathbf{g}] \tag{2}$$

Conservation of energy:

$$\Omega \frac{\partial H}{\partial t} + \nabla\cdot(\gamma_h \mathbf{u} H) = \nabla\cdot[\Gamma_h \nabla H] + \nabla\cdot\left[f(s)\frac{K\Delta\rho h_{fg}}{v_v}\,\mathbf{g}\right] \tag{3}$$

The mixture variables and properties of Eqs. (1)–(3) are defined as

density: $\rho = \rho_l s + \rho_v(1-s)$, (4)

velocity: $\rho\mathbf{u} = \rho_l \mathbf{u}_l + \rho_v \mathbf{u}_v$, (5)

pressure:

$$p = p_l + \int_0^s \lambda_v\left(\frac{\mathrm{d}p_c}{\mathrm{d}s}\right)\mathrm{d}s = p_v - \int_0^s \lambda_l\left(\frac{\mathrm{d}p_c}{\mathrm{d}s}\right)\mathrm{d}s, \tag{6}$$

enthalpy:

$$H = \rho(h - 2h_{v\mathrm{sat}}) \quad \text{with } \rho h = \rho_l s h_l + \rho_v(1-s)h_v, \tag{7}$$

kinetic density:

$$\rho_k = \rho_l[1-\beta_l(T - T_{\mathrm{sat}})]\lambda_l(s) + \rho_v[1-\beta_v(T - T_{\mathrm{sat}})]\lambda_v(s), \tag{8}$$

viscosity: $$\mu = \frac{\rho_l s + \rho_v(1-s)}{k_{rl}/v_l + k_{rv}/v_v}, \tag{9}$$

advection correction coefficient:

$$\gamma_h = \frac{[\rho_v/\rho_l(1-s)+s][h_{v\mathrm{sat}}(1+\lambda_l) - h_{l\mathrm{sat}}\lambda_l]}{(2h_{v\mathrm{sat}} - h_{l\mathrm{sat}})s + \rho_v h_{v\mathrm{sat}}(1-s)/\rho_l}, \tag{10}$$

effective heat capacitance ratio:

$$\Omega = \varepsilon + \rho_s c_s(1-\varepsilon)\frac{\mathrm{d}T}{\mathrm{d}H_l}, \tag{11}$$

effective thermal diffusion coefficient:

$$\Gamma_h = \frac{1}{1 + (1-\rho_v/\rho_l)h_{v\mathrm{sat}}/h_{fg}}\,D + k_{\mathrm{eff}}\frac{\mathrm{d}T}{\mathrm{d}H}, \tag{12}$$

capillary diffusion coefficient:

$$D(s) = \frac{\sqrt{\varepsilon K}\sigma}{\mu_l}\frac{k_{rl}k_{rv}}{(v_v/v_l)k_{rl} + k_{rv}}[-J'(s)], \tag{13}$$

relative mobility:

$$\lambda_l(s) = \frac{k_{rl}/v_l}{k_{rl}/v_l + k_{rv}/v_v}, \qquad \lambda_v(s) = \frac{k_{rv}/v_v}{k_{rl}/v_l + k_{rv}/v_v} \tag{14}$$

where the subscripts "l" and "v" denote the quantities for liquid and the vapor, respectively. The fluid temperature and liquid saturation can be recovered from the following relations:

$$T = \begin{cases} H + 2\rho_l h_{v\mathrm{sat}}/\rho_l c_l, & H \leqslant -\rho_l(2h_{v\mathrm{sat}} - h_{l\mathrm{sat}}), \\ T_{\mathrm{sat}}, & -\rho_l(2h_{v\mathrm{sat}} - h_{l\mathrm{sat}}) < H \leqslant -\rho_v h_{v\mathrm{sat}}, \\ T_{\mathrm{sat}} + \dfrac{H + \rho_v h_{v\mathrm{sat}}}{\rho_v c_v}, & -\rho_v h_{v\mathrm{sat}} < H, \end{cases} \tag{15a}$$

$$T = \begin{cases} 1 & H \leqslant -\rho_l(2h_{v\mathrm{sat}} - h_{l\mathrm{sat}}), \\ -\dfrac{H + \rho_v h_{v\mathrm{sat}}}{\rho_1 h_{fg} + (\rho_l - \rho_v)h_{v\mathrm{sat}}} & -\rho_l(2h_{v\mathrm{sat}} - h_{l\mathrm{sat}}) < H \leqslant -\rho_v h_{v\mathrm{sat}}, \\ 0 & -\rho_v h_{v\mathrm{sat}} < H. \end{cases} \tag{15b}$$

The liquid and vapor velocity can be calculated from the mixture velocity based on the following relations:

$$\rho_l \mathbf{u}_l = \lambda_l \rho \mathbf{u} + \mathbf{j}; \quad \rho_v \mathbf{u}_v = \lambda_v \rho \mathbf{u} - \mathbf{j}, \tag{16}$$

where

$$\mathbf{j} = -\rho_l D(s) \nabla s + f(s) \frac{K \Delta \rho}{\nu_v} \mathbf{g} \tag{17}$$

with the hindrance function $f(s)$ given by

$$f(s) = \frac{k_{rl} k_{rv}/\nu_l}{k_{rl}/\nu_l + k_{rv}/\nu_v}. \tag{18}$$

In this analysis, the following constitutive relationships for the relative permeabilities and the capillary pressure are used (Udell, 1985):

$$k_{rl}(s) = \left(\frac{s - s_{\mathrm{ir}}}{1 - s_{\mathrm{ir}}}\right)^3, \qquad k_{rv}(s) = \left(\frac{1 - s}{1 - s_{\mathrm{ir}}}\right)^3 \tag{19}$$

$$p_c(s) = \sqrt{\frac{\varepsilon}{K}}\, \sigma J(s), \tag{20}$$

where

$$J(s) = 1.417(1 - s) - 2.120(1 - s)^2 + 1.263(1 - s)^3. \tag{21}$$

The boundary conditions for the problem are given as follows:

at $x = 0$ and $x = W$ (vertical walls)

$$\frac{\partial p}{\partial x} = 0, \tag{22}$$

$$-\frac{\Gamma_h}{\rho} \frac{\partial H}{\partial x} = q'' \tag{23}$$

at $y = 0$ (inlet)

$$p = \rho_l g L, \tag{24}$$

$$H = \rho_l (c_l T_{\mathrm{in}} - 2h_{v\mathrm{sat}}) \tag{25}$$

at $y = L$ (outlet)

$$p = 0, \tag{26}$$

$$\frac{\partial H}{\partial y} = 0. \tag{27}$$

All the symbols used in the governing equations and the boundary conditions are defined in the Nomenclature. The pressure boundary condition given by Eq. (22) reflects that the vertical boundaries are impermeable. Eq. (24) represents the pressure boundary condition at the inlet, $\rho_l g L$ being the hydrostatic pressure due to the adjacent liquid pool, while Eq. (26) gives the outlet pressure where the hydrostatic pressure is zero. Eq. (27) represents the thermally fully developed condition for the two-phase mixture leaving the channel.

3. Numerical procedure

Before solving the energy equation given by Eq. (3), we first obtain the mixture pressure and velocity fields. To this end, we substitute Eq. (2) into Eq. (1) to obtain

$$\nabla^2 p = \frac{\nu}{K}\left[\varepsilon \frac{\partial \rho}{\partial t} - \nabla p \cdot \nabla\left(\frac{K}{\nu}\right) + \nabla \cdot \left(\frac{K}{\nu} \rho_k \mathbf{g}\right)\right]. \tag{28}$$

Eq. (28) was then discretized by the central difference method and solved using the stabilized error vector propagation (EVP) method (Wang et al., 1994). The velocity field could be subsequently obtained from Eq. (2) after the pressure field was obtained. The energy equation was solved by a fully implicit control volume-based finite difference formulation (Patankar, 1980). The temperature in the single-phase region and the liquid saturation in the two-phase region could be backed out from the enthalpy field based on Eq. (15a) and (15b). Once a converged solution was obtained, the individual phase velocities of liquid and vapor were then determined based on Eq. (16).

The equations were solved as a simultaneous set, and the solution was taken to be converged when local field values did not change by more than 0.1% in two consecutive sweeps and the residual for Eqs. (1)–(3) was below 10^{-5}. A series of test runs were performed to ensure that the numerical results were independent of the grid size. The choice of 82×44 uniform grid points was found to provide grid independence for the results reported in this paper.

4. Results and discussion

Numerical computations were carried out for a capillary porous structure of 20 mm (W) × 150 mm (L). Glass beads of different diameters d_p ranging from 0.3 to 1.2 mm were chosen as the porous media while water was selected as the working fluid. The permeability was evaluated by (Nield & Bejan, 1992)

$$K = \frac{\varepsilon^3 d_p^2}{180(1 - \varepsilon)^2}. \tag{29}$$

The effective thermal conductivity k_{eff} was calculated by using the equation by Zehner and Schlünder (1970)

$$k_{\mathrm{eff}} = k_f \left\{1 - \sqrt{1 - \varepsilon} + 2\frac{\sqrt{1 - \varepsilon}}{\Lambda B}\left[\frac{(1 - \Lambda)B}{(1 - \Lambda B)^2} \ln\left(\frac{1}{\Lambda B}\right) - \frac{B + 1}{2} - \frac{B - 1}{1 - \Lambda B}\right]\right\}, \tag{30}$$

where $\Lambda = k_f/k_s$ with k_s and k_f being the thermal conductivity of solid and liquid phases, respectively. The

Table 1
Thermophysical properties for the water–glass bead system

Property	Symbol	Solid	Liquid	Vapor	Unit
Density	ρ	2650	957.9	0.598	kg/m^3
Specific heat	c	1350	4178	1548	J/kg K
Kinetic viscosity	v	—	4.67×10^{-7}	2.012×10^{-5}	m^2/s
Expansion coefficient	β	—	5.23×10^{-4}	2.4×10^{-3}	K^{-1}
Interfacial tension	σ	—	0.0588		N/m
Latent heat of evaporation	h_{fg}	—	2.257×10^{6}		J/kg

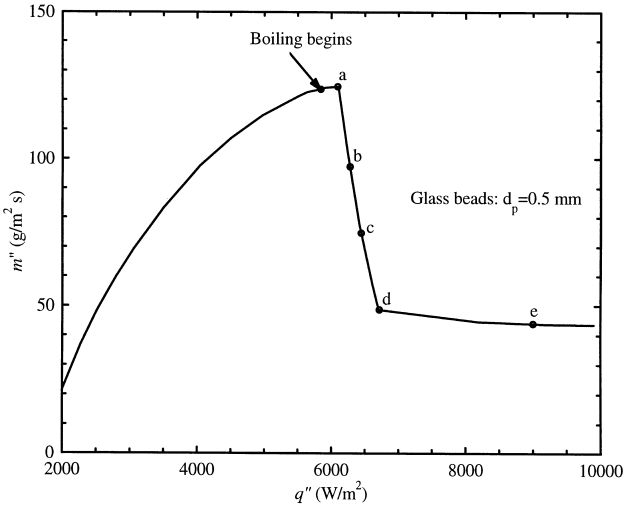

Fig. 2. The variation of the mass flux with the imposed heat flux.

shape factor B for a packed bed consisting of uniform sphere is given by

$$B = 1.25\left(\frac{1-\varepsilon}{\varepsilon}\right)^{10/9} \tag{31}$$

Other thermophysical properties for the water–glass bead system are listed in Table 1. All the computations were carried out for 1 atm pressure and at a constant inlet temperature $T_{in} = 22^{\circ}$C.

Fig. 2 presents the variation of the induced mass flux with the imposed heat flux for the glass beads of $d_p = 0.5$ mm. Before evaporation begins, the mass flux is seen to increase with the increase of the imposed heat flux. Once evaporation occurs, the mass flux continues to increase as the heat flux is further increased. However, when the heat flux exceeds about 6.1 kW/m^2, the mass flux is drastically reduced to a low value. It is also interesting to note that the mass flux remains approximately constant afterwards despite the heat flux is further increased. This interesting behavior of the variation of the induced mass flux with the imposed heat flux concurs with the result of our previous experimental study on buoyancy-induced flow with phase-change heat transfer in a vertical porous tube subjected to a uniform heat flux (Zhao, Liao & Cheng, 1998). It is relatively easy to understand that the mass flux is increased with the imposed heat flux in the single-phase flow of subcooled liquid (before the point at which evaporation begins). In this region, the motion of the working fluid within the capillary structure is solely due to the buoyancy force or the thermosyphon effect and the mass flux is proportional to the imposed heat load. In the region of the two-phase flow of liquid and vapor, one usually speculates that the mass flux would be further increased because the liquid/vapor meniscus inside the two-phase region may create a wicking effect to pump the subcooled liquid from the liquid pool into the capillary structure, in addition to the buoyancy effect. On the contrary, the experimental results showed that the mass flux drops rapidly with the increase of the imposed heat flux after evaporation occurs. In the following, we shall explain this unusual phenomenon based on the numerical results of the liquid saturation distributions as well as the vapor and liquid velocity fields at selected heat fluxes of 6.1, 6.3, 6.5, 6.7, and 9.0 kW/m^2 (corresponding to the points labeled by the letters a–e in Fig. 2).

Fig. 3 display the steady-state liquid saturation distributions in the porous channel as the imposed heat flux is progressively increased after evaporation begins, which corresponds to the points a–e in Fig. 2. It is seen from Fig. 3a that at $q'' = 6.1$ kW/m^2 (corresponding to point a in Fig. 2) an extremely narrow two-phase zone (represented by the light gray scale) is formed adjacent to the vertical walls near the exit while the capillary structure is still saturated with liquid elsewhere (representing by the dark color). Under this situation, the presence of the two-phase zone may play little role for the flow in the capillary structure simply because the zone is too small. On the other hand, the fluid temperature near the exit reaches the saturated value (100°C) and thus, the temperature difference between the inlet and the outlet reaches the maximum, implying that the buoyancy force approaches the maximum. Therefore, the mass flux at this particular heat flux reaches a peak value. As is evident from Fig. 3a and b, the two-phase zone formed near the exit of the porous channel grows quickly towards the centerline of the channel with a small

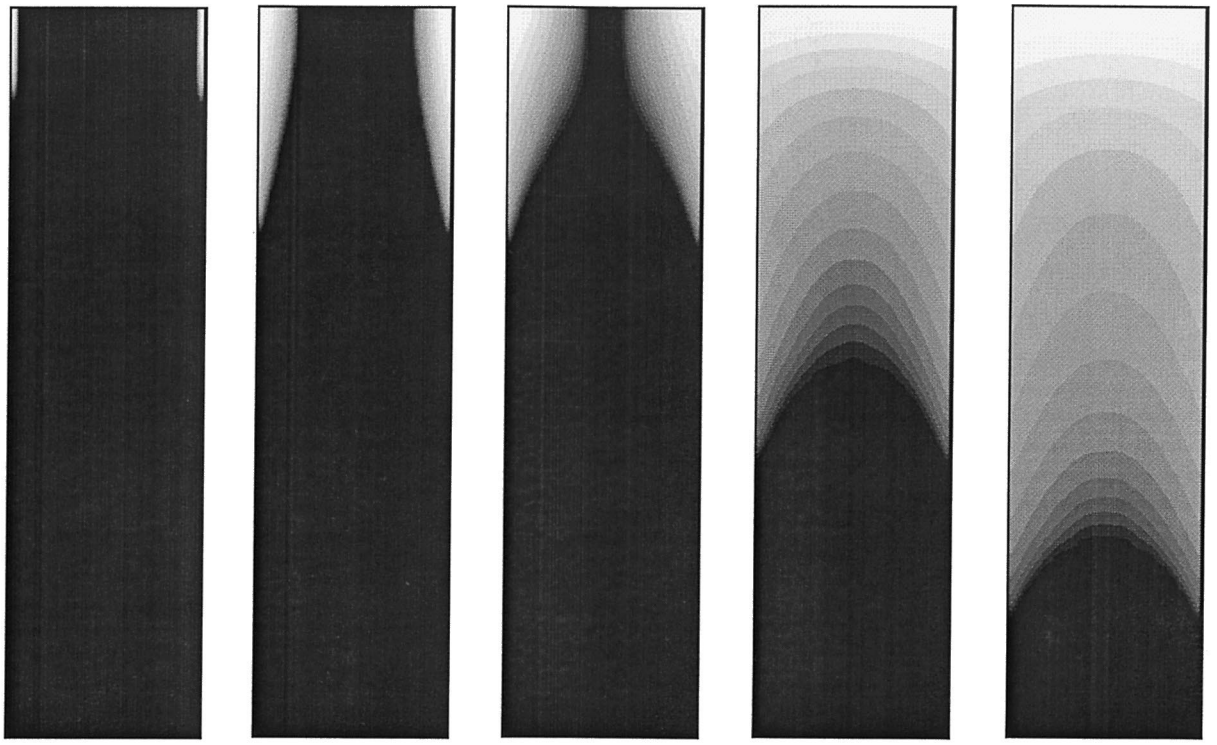

Fig. 3. The liquid saturation distributions (a) $q'' = 6.1\ \mathrm{kW/m^2}$, (b) $q'' = 6.3\ \mathrm{kW/m^2}$, (c) $q'' = 6.5\ \mathrm{kW/m^2}$, (d) $q'' = 6.7\ \mathrm{kW/m^2}$, and (e) $q'' = 9.00\ \mathrm{kW/m^2}$.

increment in the heat flux. As a result, the effect of the capillary force due to the existence of liquid/vapor meniscus on the motion of the fluid becomes more significant. However, its primary function is to draw liquid towards the heated walls but does not help much in assisting the increase of the overall mass flux in the capillary structure. On the other hand, the drag force in the two-phase zone becomes much larger than in the liquid-phase zone due to the higher viscosity of the vapor (Wang et al., 1993). A sequential scan of the liquid saturation distributions from Fig. 3a to b and c leads us to conclude that the rapid reduction of the mass flux is attributed to the fast expansion of the two-phase zone in the capillary structure as the heat flux is increased from point a to b and c (see Fig. 2). As the heat flux is further increased to point d, the two-phase zone completely fills the whole cross section of the upper region of the porous structure. As a result of vapor choking, the induced mass flux is further reduced. It is also interesting to note that the mass flux remains approximately constant despite the heat flux is increased from point d to e. This finding can be explained based on the interactions between the three major forces involved in the system such as the capillary force, the buoyancy force, and the drag forces due to the liquid and the vapor flow through the porous medium. As the heat flux is increased, both the capillary force and the buoyancy force are increased because the saturation gradient and the density difference become larger in the system. This leads to an increase of the mass flux. However, as mentioned earlier, the drag force of the vapor flow in the two-phase region also becomes rather high due to the increase of the vapor fraction. In addition, the thermal drag force (Guo & Wu, 1993) near the exit becomes relatively larger due to the lower density of the vapor in the two-phase zone, which also tends to reduce the mass flux of fluid. Therefore, the constant mass flux versus the heat flux at high heat fluxes may be attributed to the fact that the balance of the aforementioned three forces.

The velocity vectors for the flow of vapor and liquid are presented in Figs. 4 and 5, respectively. As indicated in Fig. 4a to e, vapor flows primarily upwards and away from the heated wall where the vapor is generated, and is condensed by the incoming subcooled liquid in the center part of the porous structure. A sequential examination of Fig. 4a to b shows that the underlying two-phase zone expands progressively upstream as the heat flux is increased. The liquid velocity vectors shown in Fig. 5 indicate that liquid flows primarily upwards in the most part of the cross section of the porous structure as a result of both buoyancy and capillary effects. A comparison between Figs. 4 and 5 also indicates that the near wall region, the vapor velocities are larger while the liquid velocities are smaller.

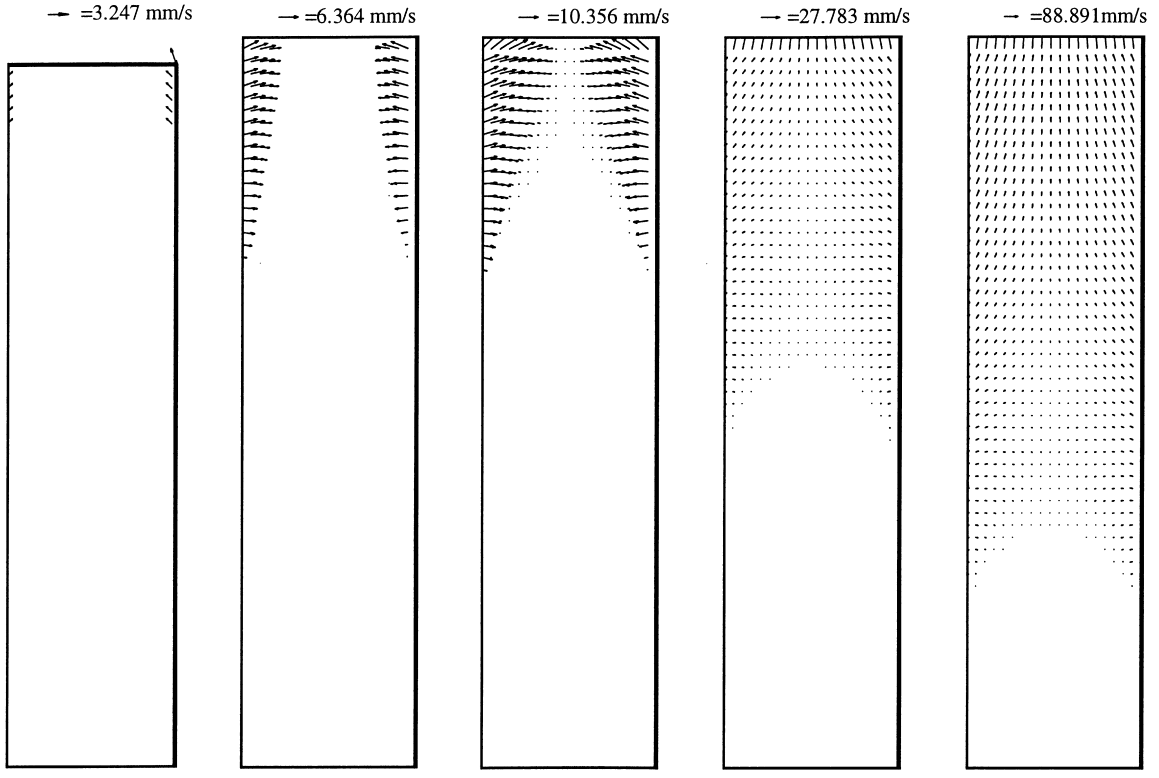

Fig. 4. The vapor velocity field at (a) $q'' = 6.1\ \mathrm{kW/m^2}$, (b) $q'' = 6.3\ \mathrm{kW/m^2}$, (c) $q'' = 6.5\ \mathrm{kW/m^2}$, (d) $q'' = 6.7\ \mathrm{kW/m^2}$, and (e) $q'' = 9.00\ \mathrm{kW/m^2}$.

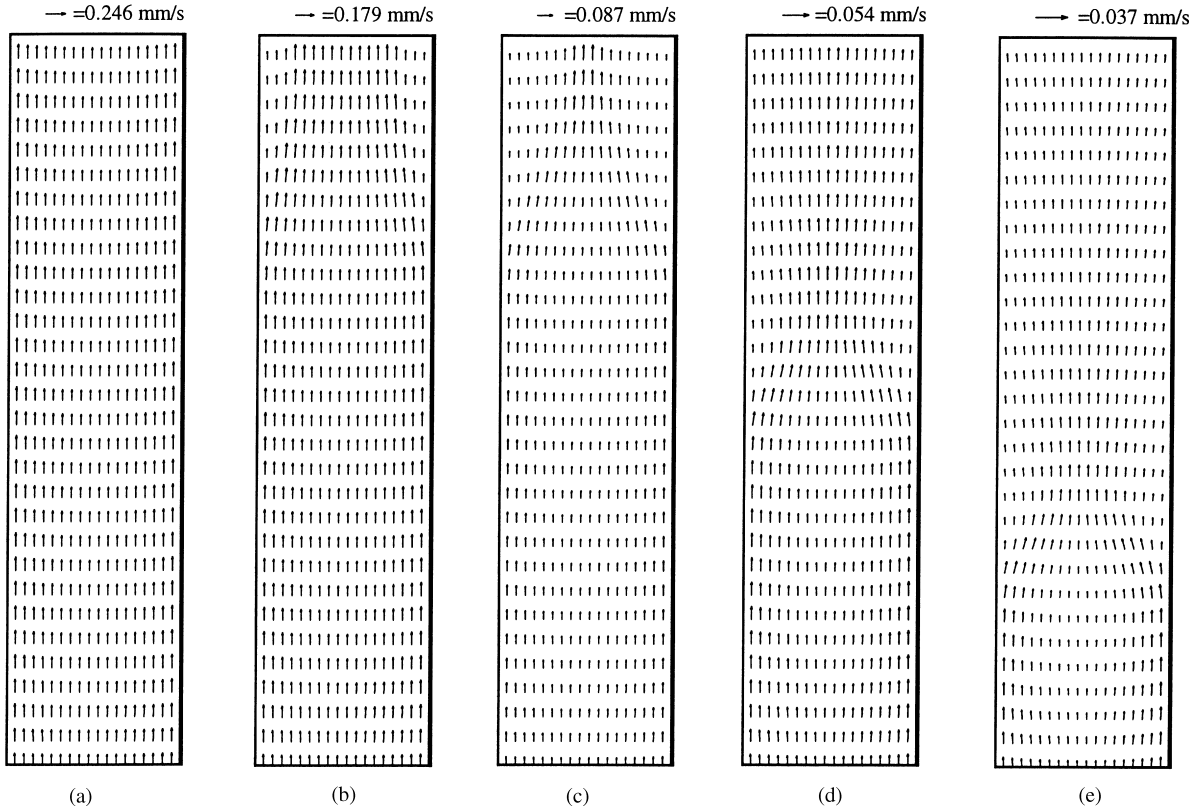

Fig. 5. The liquid velocity field at (a) $q'' = 6.1\ \mathrm{kW/m^2}$, (b) $q'' = 6.3\ \mathrm{kW/m^2}$, (c) $q'' = 6.5\ \mathrm{kW/m^2}$, (d) $q'' = 6.7\ \mathrm{kW/m^2}$, and (e) $q'' = 9.00\ \mathrm{kW/m^2}$.

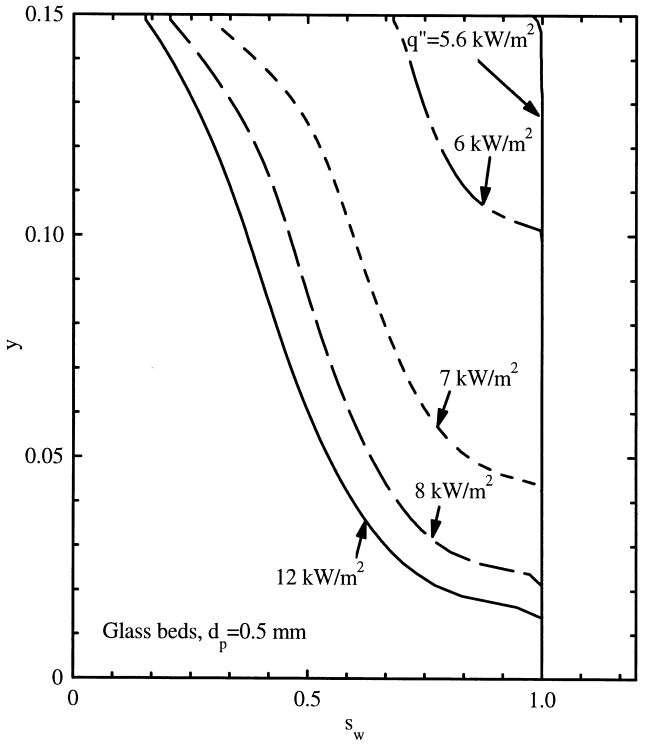

Fig. 6. The liquid saturation distribution along the heated wall at different values of heat flux.

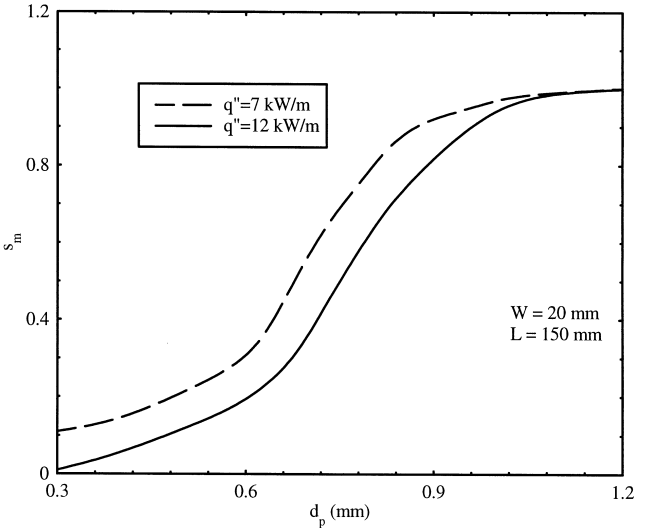

Fig. 7. The effect of the particle diameters on the minimum liquid saturation.

The variations of the liquid saturation along the heated wall for the porous medium of $d_p = 0.5$ mm at different values of heat flux are displayed in Fig. 6. It is seen that at a low heat flux of $q'' = 5.65\ \mathrm{kW/m^2}$, the liquid phase ($s_w = 1$) exists on most part of the heated surface and the liquid saturation drops slightly only near the exit of the channel. As the imposed heat flux is increased, the liquid phase region contracts while the two-phase region expands. It is evident from Fig. 6 that the liquid saturation becomes smaller along the heated wall with the increase of the imposed heat flux, reaches a minimum value at the exit of the channel for a specific heat flux. This observation implies that the dryout point always occurs at the exit of the channel for the geometry under consideration.

In order to find out the effect of the particle diameters on the dryout condition, we present the minimum liquid saturation (which occurs at the exit of the heated wall) for different particle diameters in Fig. 7. It is shown that for the same imposed heat flux, the minimum liquid saturation progressively increases with the increase of the particle diameters, indicating that a larger particle packed channel will have a higher dryout heat flux. This is mainly because that the mass flux of the subcooled liquid is affected by the particle diameters. A small particle diameter leads to a substantial increase in the drag force in the two-phase region due to higher vapor viscosity even though the capillary pressure can be increased slightly. For this reason, the mass flux of the subcooled liquid is increased with the increase of the particle diameter. Thus, the channel packed with larger particles gives a higher dryout heat flux.

5. Concluding remarks

A numerical solution has been obtained for a buoyancy-induced flow and phase-change heat transfer in a capillary structure heated symmetrically along its vertical walls. Liquid saturation distributions and the velocity fields for both vapor and liquid in the porous column are analyzed and presented. It is shown that for both single- and the two-phase flow with a rather low vapor fraction, the induced mass flux increases as the applied heat flux is increased. However, as the vapor fraction is increased further, the induced mass flux drops drastically and remains approximately constant afterwards, although the heat flux is further increased. This finding is in agreement with the results of our previous experimental study on phase-change heat transfer in a heated vertical porous tube (Zhao et al., 1998). The numerical results indicate that vapor-choking is responsible for the rapid reduction in the mass flux. It has also been shown that the dryout point always occurs at the wall near the exit of the packed channel and that larger particles give higher dryout heat flux.

Acknowledgements

This work was supported by a Hong Kong RGC Earmarked Research Grants No. HKUST 6045/97E and No. HKUST 814/96E.

References

Bear, J. (1972). *Dynamics of fluids in porous media*. New York: Elsevier.

Easterday, O. T., Wang, C. Y., & Cheng, P. (1995). A numerical and experimental study of two-phase flow and heat transfer in a porous formation with localized heating from below. ASME Heat Transfer and Fluid Engineering Divisions, HTD 321 (pp. 723–732).

Guo, Z. Y., & Wu, X. B. (1993). Thermal drag and critical heat flux for natural convection of air in vertical parallel plates. *ASME Journal of Heat Transfer*, *115*, 124–129.

Nield, D. A., & Bejan, A. (1992). *Convection in porous media*. New York: Springer-Verlag.

Patankar, S. V. (1980). *Numerical heat transfer and fluid flow*. New York: Hemisphere.

Peterson, G. P., & Chang, C. S. (1998). Two-phase heat dissipation utilizing porous-channels of high-conductivity material. *ASME Journal of Heat Transfer*, *120*(1), 243–252.

Ramesh, P. S., & Torrance, K. E. (1990). Numerical algorithm for problems involving boiling and natural convection in porous materials. *Numerical Heat Transfer B*, *17*, 1–14.

Udell, K. S. (1985). Heat transfer in porous media considering phase change and capillary — the heat pipe effect. *International Journal of Heat Mass Transfer*, *28*, 485–495.

Wang, C. Y. (1996). Modeling of capillary evaporators. In *Proceedings of the international conference on porous media and their applications in science, engineering and industry* (pp. 602–627). Hawaii: Kona.

Wang, C. Y., Beckermann, C., & Fan, C. (1993). A new approach to two-phase transport in porous media: two-phase mixture model. ASME Heat Transfer and Fluid Engineering Divisions. HTD *173, 265* (pp. 1–13).

Wang, C. Y., Beckermann, C., & Fan, C. (1994). Numerical study of boiling and natural convection in capillary porous media using the two-phase mixture model. *Numerical Heat Transfer A*, *26*, 375–398.

Wang, C. Y., & Cheng, P. (1997). Multiphase flow and heat transfer in porous media. *Advances in Heat Transfer*, *30*, 93–196.

Zehner, P., & Schlünder, E. U. (1970). Thermal conductivity of granular materials at moderate temperatures. *Chemie Ingenieur Technik*, *42*(14), 933–941.

Zhao, T. S., Liao, Q., & Cheng, P. (1998). An experimental study on variations of buoyancy-induced mass flux from single-phase to two-phase flow in a vertical porous tube. *ASME Journal of Heat Transfer*, *121*(3), 646–652.